Chapter 4. Three-dimensional thermohaline approach

Two-dimensional thermohaline simulations derived from a cross section through the NEGB provided convincing evidence for the existence of regional convective flow throughout the basin. The results have revealed that salty subsurface flow can be driven by thermally induced convection. However, it remained unclear whether the convective regime will be stable in three dimensions and to which degree the convection cells are directly related to salt structures. Moreover, a two-dimensional analysis alone is not sufficient to derive the observed solute distribution at the surface.

In this chapter, a three-dimensional analysis is attempted in order to further clarify which mechanisms underlie salt transport in the NEGB. 3D thermohaline simulations are carried out for two different scenarios. In the first part, a large scale regional model (230x330 km) indicates that salt water occurs close to the surface within the lowlands along the larger rivers. However, the coarse mesh resolution does not allow to quantify temperature effects on the mass distribution. In the second part, a smaller-scale model (10x10 km) is constructed with a grid resolution accounting for possible thermally induced convective flow. Initial and boundary conditions are those used in the two dimensional approach.

4.1 Large-scale model scenario

The study area covers 230 x 330 km in the horizontal and 5 km in the vertical direction (cf Chapter 1). The model scenario has been subdivided into a 3D finite-element mesh composed of triangular prisms. The defined grid provides an horizontal cell resolution of approximately 2.5 x 2.5 km while the vertical resolution is variable depending on the thickness of the layers. 340,000 grid points are used to discretize the balance equations of the numerical model. The mesh allows to incorporate the geological model (Scheck 1997; Scheck and Bayer 1999) into the FEFLOW database. Furthermore, the resolution ensures to keep computational time at a reasonable level in solving the bulk calculations. The choice of triangular cells has been dictated by the need for adapting the grid to the irregular shape of the natural boundary conditions imposed by the northern coast line and the basin margins. Especially at the southern margin the sedimentary fill does not exceed a total thickness of 40 m as shown schematically in Fig. 4.1. These regions correspond to eroded layers where fluid flow and mass transport play a minor role. In order to represent these no-flow zones in the numerical

model and to preserve the 3D geological structure, as well as the natural boundary conditions, very low permeability and diffusivity values (close to zero) are assigned throughout the uplifted area. Hence, in such areas, the calculated flow rates are almost equal to zero.

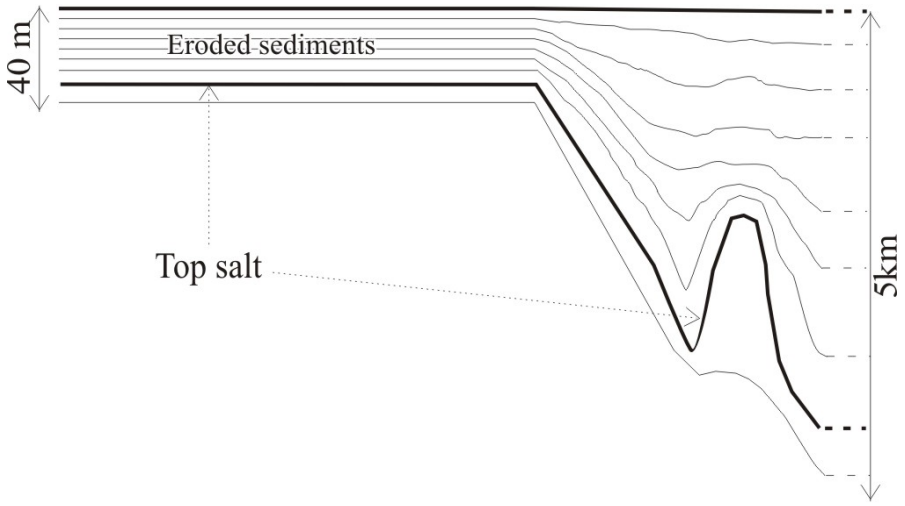

Fig.4-1: Sketch of the geological structure near the uplifted area.

Fig.4-2 illustrates the calculated salinity of the pore water at the surface at the end of the simulation run. The results indicate two wide areas where dissolved halite reaches the surface. A first plume extends over 100 km approximately, from the western limit of the study area to the southern basin margin while the other develops west of Berlin stretching over 140 km in the north-south direction. Few isolated and smaller patterns of salty water which reaches the surface (of the order of 10 km length) can also be observed along the Elbe river between the two main plumes and close to Berlin.

The calculated mass concentrations ranges from fresh water (0 g/l) to solute values (1.5 g/l), which are in good agreement with field measurements. The highest salt concentrations can be observed in the south-western area, near the basin margin. The concentration range provided by the numerical calculations points towards the existence of intrinsic system dynamics, such as upward saline flow.

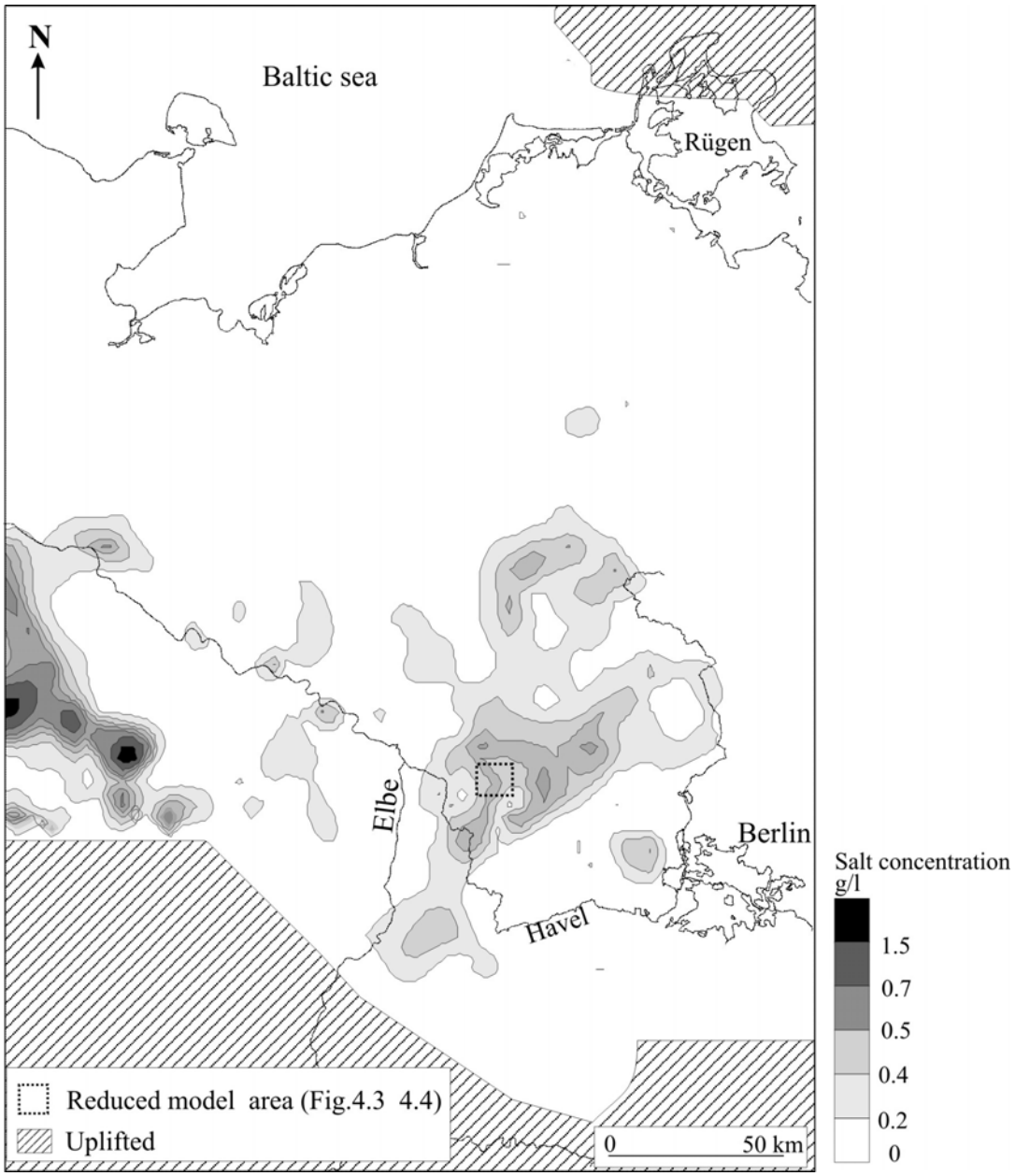

Fig.4-2: Large scale model scenario results. Calculated mass distribution at the surface at the end of the simulation run.

A comparison of Fig.1-1 (Chapter 1) with Fig.4-2 reveals similarities between the calculated salinity plumes at the surface (Fig.4-2) and the saline groundwater distribution as compiled by Grube et al. (2000) (Fig.1-1). In particular, in the south-western area (from the Elbe river to the basin margin) and in the central part of the basin the calculated brine patterns (Fig.4-2) are in agreement with the observed data (Fig.1-1). The data compiled by Grube et al. (2000) account for groundwater salinity profiles from the surface to a depth of 300 m whereas the numerical model provides solute distribution at the surface. Therefore the areas of Fig.4-2 which do not compare favourably with the data map (Fig.1-1) likely correspond to the occurrence of brines at deeper levels. Observations as well as modelling results indicate that

hydrostatic flow probably provides the dominant mechanism in the lowlands along the Elbe river.

Simulations of coupled fluid flow and solute transport, provides similar surface brine patterns obtained from the thermohaline simulations. The reason is that the selected grid resolution is not fine enough to account for thermohaline effects. In order to quantify temperature effects on the calculated solutal gradients, a higher cell resolution is required. Further mesh refinements have revealed a dramatical increase in computational time for the bulk calculations of the numerical balance equations. Therefore within the given modelling framework, a higher density of active nodes discretizing the large scale model cannot be realised together with long time simulations. Consequently, it is necessary to reduce the area of the study model in order to define a highly refined grid adapted to thermohaline convective flow.

4.2 Square box model scenario

The location of the detailed model is indicated in Fig.4-2. The area covers a square box of 10 km length. The location has been chosen because it is situated within one of the identified surface brine plumes, as shown in Fig.4-2. Fig.4-3 illustrates the topography of the study area without significant topographical variation. Consequently, hydrostatically driven flow should not be the primary force. Moreover, in this site, no diapir is present. Therefore, sub-surface brine occurrences are not related to strong lateral salinity gradients supplied by salt diapirs.

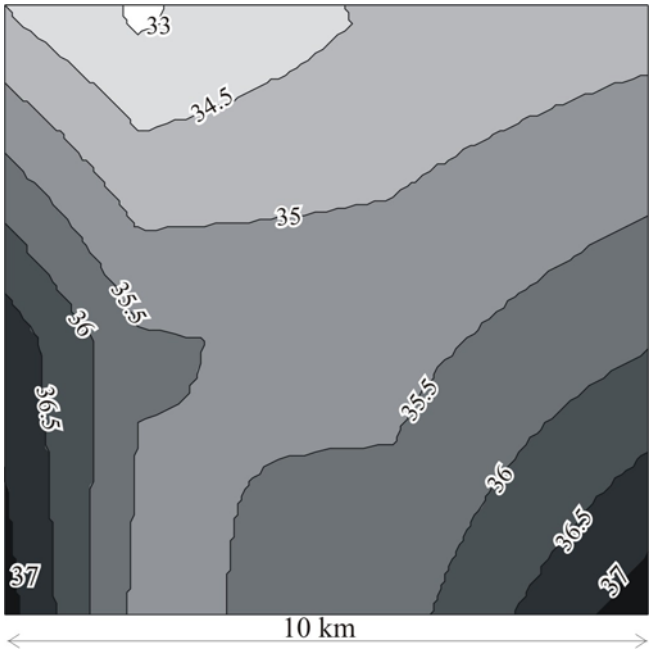

Fig.4-3: Topography (m) of the reduced model scenario

The domain has been subdivided into a rectangular mesh containing 34 x 34 grid points, resulting in a cell resolution of 290 m.

In order to provide an evolution analysis, the simulation results will be illustrated for two time steps. Solutions of the coupled balance equations will be shown at a computing time of 30 ka and at the end of the simulation run (200 ka).

Fig.4-4 shows the calculated solute (g/L) and temperature (°C) distribution at the surface of the model area at t = 30 ka (A) and at the end of the simulation run (B). Solute and thermal plumes occur at the surface occupying identical regions. As time progresses, the plumes persist, however, they stretch over a longer distance. Particularly, higher salt concentrations correlate with increased surface temperature.

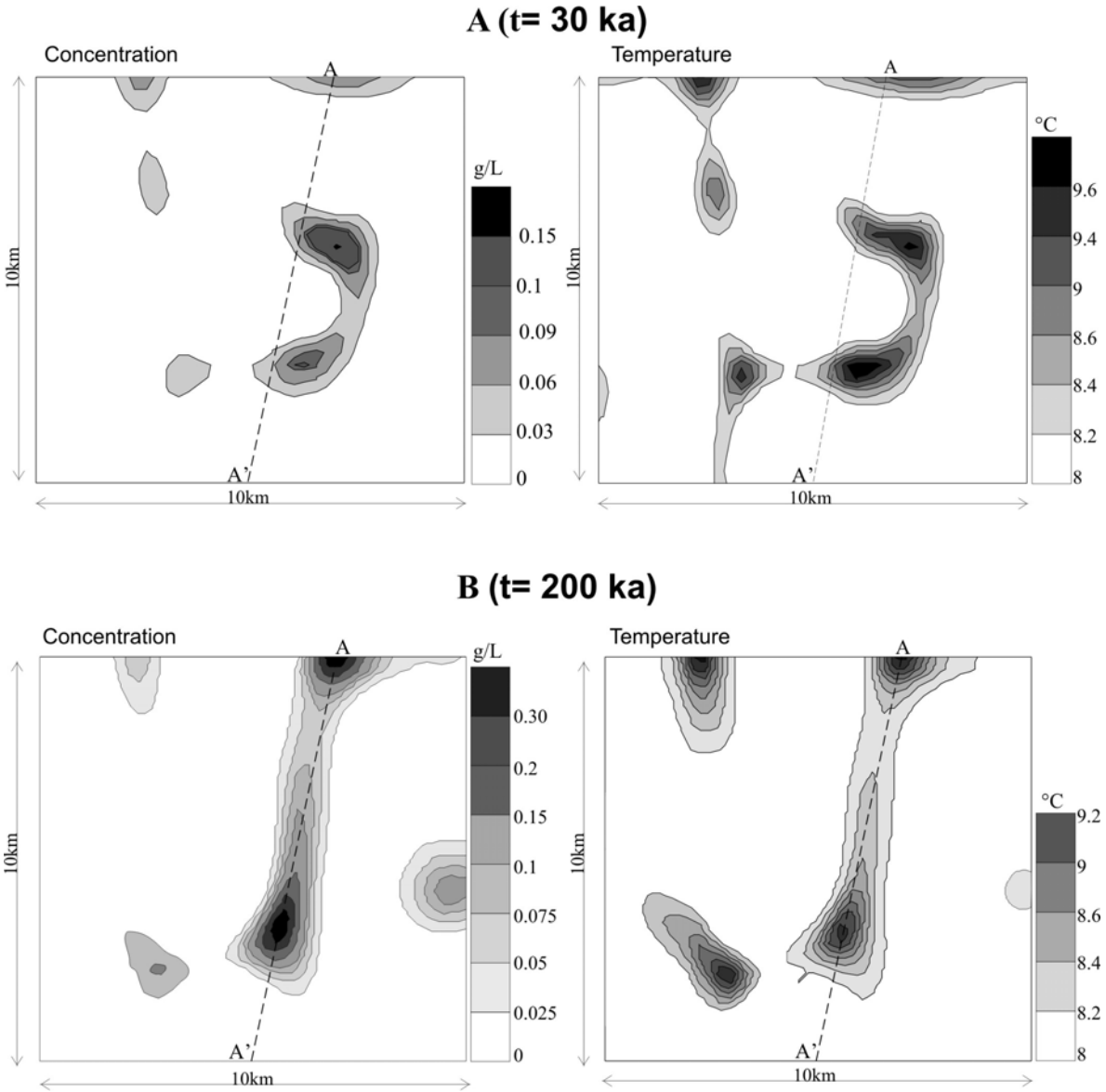

Fig.4-4: Reduced model scenario results. **A:** Calculated patterns at the surface at t = 30 ka and **B** at t = 200 ka respectively. Left: salt distribution (g/L). Right: temperature (°C) distribution at the surface. Dotted lines indicate the location of the selected cross-section A-A'.

These simulations highlight two significant aspects of the flow regime:

- If the temperature input is removed from the numerical calculations, no saline water reaches the surface.
- The peak concentration calculated at the end of the simulation run is two times higher than the concentration observed at the onset of the process. The temperatures approximately span the same range.

These two features of the system can be explained as follows. Without temperature input no solute plumes develop, therefore it can be inferred that thermal effects on fluid density generate buoyant forces strong enough to overcome the gravity field that keeps heavy brine close to the salt layer. Consequently, as time progresses, the brine undergoes a continuous salt replenishment from below by upward solute transport induced by the temperature gradient. This process leads to higher concentrations at the surface at the end of the simulation run. In summary, these results indicate that the deep-seated brine can locally reach the surface driven by induced free thermohaline convective flows even in absence of steep salt diapirs. However, the salt concentration values at the surface are inferior to those calculated from the 2D simulations.

In order to emphasize the mechanisms driving solute up to the surface, the calculated concentration, temperature and velocity field are extracted at each computing time step along a cross-section (denoted by A-A' in Fig.4-4). The section of approximately 9,5 km length slices the main brine and temperature pattern obtained at the surface at the end of the 3D simulation run (Fig.4-4 B). In Fig.4-5 the geological structure along A-A' as well as the finite element mesh are shown.

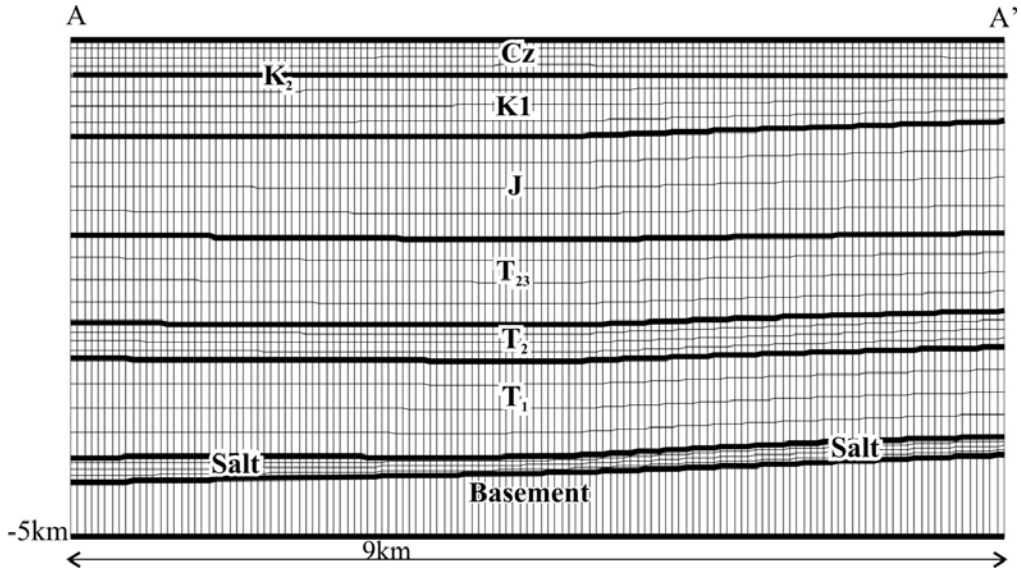

Fig.4-5: **A)** Geological structure (abbreviations given in Table.1) and finite element mesh of the selected cross-section as shown in Fig.4-4.

Fig. 4.6 1, 2, 3 illustrate the calculated velocity (m/yr^{-1}), mass (g/L), and temperature (°C) distribution at a computing time of 30 ka (A) and at the end of the simulation run (B).

Fig.4-6. A1 shows the calculated pore velocities of the convective cells at t = 30 ka. Vectors indicate the flow directions. The velocity values range from 37 cm per year in the shallow aquifer to few millimeters per year in the deeper stratigraphic units. The vigour of convective flow decreases of ten orders with increasing depth. This strong velocity contrast is due to the vertical heterogeneity of the layers within the system. Indeed, the shallow aquifer consists of layers which have the highest permeabilities (Table.1). This velocity feature is also confirmed by Rosenberg and Spera (1990) who investigated the role of layered permeability heterogeneity in hydrothermal convection.

The flow dynamics, thereby, separates into two subsystems (Fig.4-6 A2):

1: Above the Muschelkalk (located at 3 km of depth), the upward flow is associated with convective transport of dissolved salt which is manifested as salinity plumes protruding throughout the sediments up to the surface. Brine plumes develop as three separated streams forming two well-defined vertically stacked convective cells. The flow field characteristics, described here, are in agreement with those derived from theoretical considerations by Rosenberg and Spera (1992). In that study, the authors summarized the various types of dynamics occurring in thermohaline convection in a porous medium heated from below for different sets of initial conditions and buoyancy ratios. The model scenario presented here corresponds to what they define a “salted from below” boundary condition and “layered box” initial condition system at high buoyancy ratio. For this particular configuration, Rosenberg and Spera found that at early computing time the flow field consists of vertically stacked convection cells. Here , the plumes crests are spaced at about 3 km in the horizontal direction.

2: Below the Muschelkalk (within the Buntsandstein) the mass transfer is dominated by diffusion. Accordingly, the solute concentration field is not disturbed presenting almost flat isopleths. The interface fresh water/brine is approximately located at 3 km below the surface within the Muschelkalk.

Fig.4-6 A3 shows the same system dynamic in terms of heat transfer: above the Muschelkalk the heat transfer is characterized by protruding plumes reaching the surface locally while at deeper levels heat transfer is dominated by conduction.

By comparing Fig.4-6 A2 with Fig.4-6 A3, it results that the “density lid” described in the 2D thermohaline simulations is preserved even in 3D: heat and brine plumes rise together to approximately the same height.

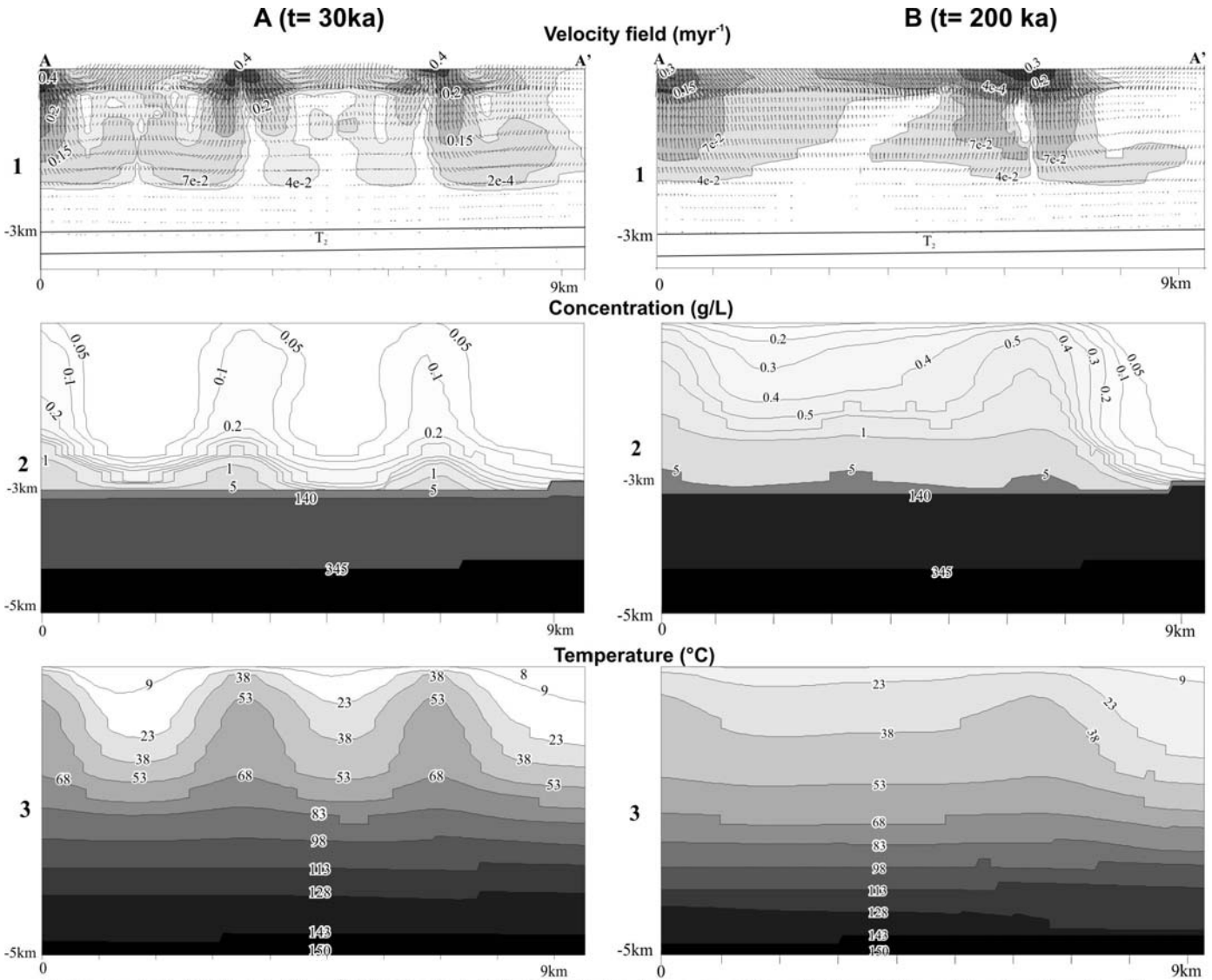

Fig.4-6: **1)** velocity field along A-A' (myr^{-1}) **2)** Profile of salt distribution (g/L), **3)** and temperature (°C) resulting from 3D thermohaline simulations at t = 30 ka.(A) and at t = 200 ka

A comparison of Fig.4-6 A1 with 4.6 A2 and with Fig.4-6 A3 emphasizes the strong relation between the vigour of upward convective flows and the areas where thermal and solute plumes protrude. Salty water locally reaches the surface where the highest values of temperature and flow velocity are observed.

At the end of the simulation run (Fig.4-6 B), the system approaches a steady-state which is favored by the lateral boundary conditions. This feature is once more confirmed by Rosenberg and Spera (1992); the authors predicted that, for this type of model scenario, the vertical stacked cells observed at early simulation time eventually evolve to a steady-state. Although the pattern simplifies, the flow regimes still persist. The final flow velocities show still higher values in the shallow aquifer, and peak velocity values are observed in those locations of the study area where solute and thermal plumes reach the surface. The convection pattern is still penetrative but presents only one and a halve weak cell. Above the Muschelkalk concentration and temperature gradients are disturbed by the convective regime while below this stratigraphic unit solute and heat transfer are conductive.

Comparison of Fig.4-6 B2 with Fig.4-6 B3 shows that the feature of the density lid is still preserved: the highest solute concentrations are at the top of the convection cell at the same height of the heat plumes. From these pictures, it can also be noticed that the density lid promotes lateral flow of the plumes toward A'.

By comparing Fig.4-6 A with Fig.4-6 B, the velocities have slightly decreased as more solute is advected in the shallow aquifer by the upward convective flows. Some of the weaker convective cells are swallowed up by stronger neighbouring cells. Ranganathan and Hanor (1988) found the same behavior for pore velocities near salt domes. At the end of the simulation run high concentration isopleths come closer to the surface than in earlier phases of the process. Consequently, the sediments above the Muschelkalk are almost all filled with brine and higher concentration values can be observed locally at the basin surface.

In summary, the highly refined grid defined for the reduced model scenario allows to account for thermohaline effects. Simulation results prove that temperature effects on fluid density provide buoyancy forces strong enough to generate upward flows driving dissolved halite to the surface even in absence of steep salt diapirs.

Cross-sections of the calculated 3D pattern provide additional insight into the dynamic of the resulting thermally induced flows. Specifically, two major features are found to persist: above the Muschelkalk the vigour of flow is higher and is manifested by convective cells developing within the sediment fill. On the other hand, below this layer, the system regime is purely conductive. Furthermore, 3D thermohaline simulations emphasize the strong link

between concentration and temperature distribution. In both horizontal and vertical direction, thermal and solute plumes always correlate in space and time.

Evolution analysis of the calculated profiles show that, supported by the close boundaries, dissolved solute continues to fill the shallow aquifer from below as time progresses. Consequently, the increasing concentrations weaken the convective cells. Nevertheless, even in the presence of high dissolution rates, the disturbed temperature gradient generates velocity fields able to drive solute locally up to the surface.

4.3 Discussion

3D numerical simulations of coupled fluid flow, heat and salt transport correlate with the observed data. The large model scenario indicates that regional flow is one mechanism driving solute within the basin. Wide stretched salty plumes spread at the surface even without temperature input. The highly refined model scenario additionally accounts for thermohaline effects on the system dynamics. It was found that the patterns are stable even in three dimensions and that the flow regime strongly depends on the basin lithology. Above the Muschelkalk, plumes of dissolved salt protrude throughout the sediments fill and reach the surface locally, whereas conductive heat and solute transport dominates the deeper part of the basin. The reduced model scenario emphasizes that even without salt diapirs the temperature gradient can be disturbed. Consequently upward solute transport is also possible above flat salt structures due to the resulting thermally induced flow. However, the salt concentration values at the surface are inferior of those calculated from 2D modeling in which salt diapirs are included.

Therefore hydrostatically driven fluid flow and thermohaline convection can be considered among the major mechanisms currently affecting parts of the NEGB, probably even supplying the observed saline springs. The modeling results already provide strong indication that regional flow and temperature-driven convective flow play an important role in driving solute within the area under consideration.